

Computer Enabled Design Optimisation of Heat Exchanger Systems for Next Generation Aerospace Vehicles

MECH5080M Team 94:
*Computer Enabled Design
Optimisation of Heat Exchanger
Systems for Next Generation
Aerospace Vehicles*
Supervisor: Harvey Thompson
Industrial Mentor: Shahrokh
Examiner: Carl Gilkeson
Date Submitted: 30/04/2024

MECH5080M TEAM PROJECT 45 credits

TITLE OF PROJECT

Computer Enabled Design Optimisation of Heat Exchanger Systems for Next Generation Aerospace Vehicles

PRESENTED BY

Daniel Nixon, Aaron Racher, Ellie Christensen & Liam Huckle

OBJECTIVES OF PROJECT

1. Review literature on the optimisation of cold plates.
2. Build a validated 3D CFD conjugate heat transfer model & analytical model of a serpentine channel cold plate.
3. Construct initial DoE and run simulations analytical model.
4. Build fully parameterised 3D CFD model of baseline geometry.
5. Reduce design space and run simulations of refined DoE with CFD model.
6. Construct surrogate model and use machine learning as a tool for validation.
7. Run multi objective optimisation algorithm on the surrogate model to identify optimal design parameters.
8. Evaluate the Pareto front, examining its applicability to industry.

IF THE PROJECT IS INDUSTRIALLY LINKED TICK THIS BOX
AND PROVIDE DETAILS BELOW

X

COMPANY NAME AND ADDRESS:

Kings Place, 3rd Floor 90 York Way, London, N1 9FX

INDUSTRIAL MENTOR: Shahrokh Shahpar

THIS PROJECT REPORT PRESENTS OUR OWN WORK AND DOES NOT CONTAIN ANY UNACKNOWLEDGED WORK FROM ANY OTHER SOURCES.

NAME

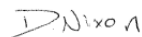
Daniel Nixon

Aaron Racher

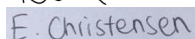
Ellie Christensen

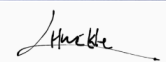
Liam Huckle

SIGNED









DATE

26/04/2024

26/04/2024

26/04/2024

26/04/2024

MULTI OBJECTIVE DESIGN OPTIMISATION OF HEAT EXCHANGER SYSTEMS FOR NEXT GENERATION AEROSPACE VEHICLES

Daniel Nixon, Aaron Racher, Ellie Christensen
& Liam Huckle

ABSTRACT

The aviation sector significantly contributes to global carbon dioxide emissions and has thus established a target of achieving net zero emissions by 2050. This ambitious goal demands innovative electrical frameworks that produces significant waste heat, calling for highly effective thermal management. Rolls-Royce has introduced a foundational serpentine channel cold plate geometry, offering a promising design that achieves an optimal balance between efficiency and heat transfer maximisation. In this report, a 3-design variable (channel diameter, corner radius, and Reynolds number) optimisation workflow is used with the objectives of minimising both thermal resistance and pressure loss. A lower fidelity analytical model is used to investigate an initial large design space, which is then refined and ran using a higher fidelity Computational Fluid Dynamics (CFD) model. The data generated is employed to build surrogate models, facilitating a comprehensive understanding of the interaction within the design spaces. Single-objective optimisation algorithms applied to these models uncover that both objectives exhibit greater sensitivity to flow rate rather than geometry. The implementation of multi-objective optimisation and thus the establishment of a Pareto front equips designers with a set of optimal solutions that effectively balance each objective through trade-offs. The optimal design found yielded a 49.0% and 13.8% decrease in pressure drop and peak baseplate temperature, respectively.

Keywords – CFD, optimisation, thermal resistance, pressure drop.

1. INTRODUCTION

In 2022, aviation contributed to 2% of global energy-related CO₂ emissions, exhibiting a more rapid growth in recent decades compared to rail, road, or shipping [1]. Nonetheless, the global aviation industry has committed to striving for net-zero emissions by 2050 [2]. In pursuit of this goal, a key aspiration of the aviation sector involves outfitting

aircraft with electric propulsion systems fuelled by either batteries or hydrogen fuel cells [3]. The development of the modern All-Electric Aircraft necessitates the creation of a novel electrical framework [4]. These electrical systems generate significant amounts of waste heat at low temperatures, [5] thus requiring sufficient cooling to prevent severe issues (efficiency losses and performance degradation) for electrical components [6]. Yet, the total heat sinks available on board are significantly constrained by weight limitations, posing a risk to the longevity of the on-board equipment, and potentially compromising the entire flight system, as well as reducing the vehicle's flight time and range [7]. Consequently, heatsink design and thermal management are integral to the design process [8].

A popular heatsink design is serpentine channel cold plates which are gaining popularity as a thermal management option due to their high heat transfer coefficient and potential to be used in high heat flux applications [9] [10]. They are particularly suitable for aviation due to their compactness and lightweight nature, which is a driving design criterion on aircraft [11]. The baseline geometry provided by Rolls Royce which has been optimised in this report is displayed in figure 1.1.

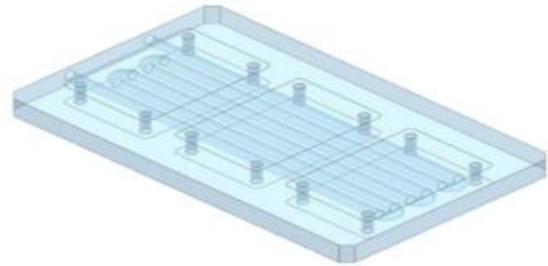


Figure 1.1: Diagram of baseline cold plate geometry provided by Rolls Royce.

This design comprises of a rectangular aluminium cold plate, with three sets of 180 degree turning serpentine channels, and two sets of heat sources consisting of three-square plates each. A typical serpentine channel heat sink comprises of a metal base plate with a serpentine channel where a fluid coolant moves from the inlet, through the channel and out of the outlet. These heat sinks have a uniform flow distribution which gives them advantage over parallel channel heat sinks which have a non-uniform flow distribution which can be detrimental to heat transfer [9]. In serpentine channel configurations heat transfer performance is further enhanced by the channel bends which cause flow separation and recirculation of the coolant, resulting in interruptions in the thermal boundary layer, thus increasing the rate of heat transfer [9]. Often water is used as the coolant due to its enhanced heat transfer properties when compared to air [12] but a number of nanofluids can

also be used [10]. The coolant mixture suggested by Rolls Royce is water and Ethylene –Glycol mixture.

Literature highlights several studies which investigate and optimise the design of a serpentine channel heatsink. Al-Neama [13] presents a study where the channel width, number of channels and chevron oblique angle are optimised to minimise the pressure drop and thermal resistance of the heatsink. Li et al. [14] investigated the aspect ratio of the serpentine channels and the ratio of fin width to channel width also for minimising both pressure drop and thermal resistance. Ismaeel et al. [15] introduced secondary colling channels to further improve heatsink operation, the study focuses on the main channel width, secondary channel length and the oblique angle of the fins to restrict thermal resistance and pressure losses. All studies show how impactful heatsink design can be on the overall performance of a heatsink. The work presented in this paper investigates and proposes to optimise the Reynolds number of the flow; the serpentine pipe diameter; the radius of the bend of the serpentine, with the objective of minimising both pressure drop and thermal resistance. Studies in this field are extensive, however the coupled effect of flow rate and geometry has not been considered. The paper aims to explore this gap in the field and propose an optimised geometric design for an optimised Reynolds number or flow rate.

One method of investigating the performance of cold plate designs is analytical modelling. This is a low fidelity method, which utilises thermodynamic and fluid mechanics equations, along with correlations derived from numerical investigations, in a basic coding software, such as MATLAB, but can provide results that are in good agreement with higher fidelity simulations [16]. Due to its low computational requirements, it is highly compatible with optimisation methodologies, as it can run hundreds of design points rapidly [17]. There are many assumptions that are required to model analytically, detailed in chapter 2. Therefore, its applicability is limited to more basic repetitive geometry where it is restricted to providing low resolution temperature and pressure information, generally producing an average value for fluid temperature and pressure drop per channel.

Imran et al. [10] successfully used CFD to simulate different microchannel serpentine cold plate designs to assist in analysing the optimal microchannel serpentine design. This investigation highlights one of the benefits of CFD compared to analytical models; CFD can be explicitly tailored to intricate designs, and with a range of boundary conditions it can produce results with a great level of accuracy. The drawback of CFD is that it will take

more time to calculate than analytical methods especially if the case scenario is very complex and has a high-resolution mesh.

Through computational tools like MATLAB, a systematic exploration of the multidimensional design space is conducted using a Design of Experiments (DoE) approach. The optimisation problem is defined to minimise both thermal resistance and pressure drop while adhering to geometric constraints as well as performance criterion. Leveraging Morris Mitchell Latin Hypercube Sampling (LHS), a comprehensive dataset is constructed which adheres to creating a space filling non collapsing design space outlined in DoE theory [18]. Surrogate models are trained on data from both analytical methods and CFD, these models approximate the real model across the entire design space [19]. This approach accelerates the exploration of the design space, facilitating streamlined optimisation efforts.

Several single objective optimisations are conducted on these metamodels to ascertain an understanding into the dependency of different design variables on the investigated objectives. This information is then used to inform a multi-objective optimisation using multi-objective genetic algorithms (MOGAs). MOGAs are widely recognized as a popular optimisation algorithm, especially well-suited for addressing multiple conflicting objectives [20]. The genetic algorithm will produce an entire Pareto optimal solution set or a representative subset, this comprises of solutions that are non-dominated relative to one another [20]. Decision makers can utilise this front as a tool for trading off the pressure drop and the thermal resistance, essentially leading to an enhanced serpentine channel heatsink respective to their needs.

This report aims to optimise a baseline geometry serpentine channel heatsink which is used for cooling high powered batteries. The structure of the report is as follows; after the introduction, the analytical and CFD model development is detailed, in chapter 2 and 3 respectively. Next, the validation approach and data are covered in chapter 4. Chapter 5 covers the workflow utilised for the optimisation, as well as all results obtained. This then leads into the discussion of the results and Pareto front obtained in chapter 6. Finally, the report will conclude our findings and suggest areas for future work.

2. ANALYTICAL MODELLING

In this section, the series of equations and correlations utilised within the analytical model, as well as all assumptions made during the model development (in MATLAB), are detailed in full.

2.1 Pressure Drop

The pressure loss throughout the serpentine channel cold plate is calculated as the sum of losses due to friction in the straight channel sections and losses around the bends, as shown in equation 2.1.

$$\Delta P = \frac{1}{2} \rho U_{in}^2 \left[\left(4i f_{app} \frac{L_{ch}}{D_h} \right) + \left(\sum_1^{i-1} K_b \right) \right] \quad (2.1)$$

where ΔP is pressure drop, ρ is the fluid density, U_{in} is the fluid inlet velocity, i is the number of channels, f_{app} is the average friction factor in the straight channel sections, D_h is the hydraulic diameter of the channel, L_{ch} is the length of the straight channel segments, and K_b is the pressure loss coefficient for each individual bend. For calculating the loss around the bends, Maharudrayya [21] developed a laminar flow correlation, which is applicable when the geometry of the heatsink meets the following criteria:

Table 2.1: Geometric parameter ranges of validity for analytical equations.

Aspect Ratio	Width Ratio	Curvature Ratio
$1 < a < 6$	$1 < b < 30$	$0 < C < 6$

There are 3 ranges of Reynolds number for which the equation used to determine the excess loss coefficient is different. When combined, the total range of Reynolds number for which the correlation is valid is $0 < Re < 2200$. Together, this range of Reynolds number along with table 2.1 and additional information directly inform the feasible design space. The specific ranges for the design variables in the initial design space is detailed in table 2.2. For additional information on how each range was determined, and more information on pressure loss equations, refer to [22].

Table 2.2: Initial design space variable ranges.

Reynolds Number	Channel Diameter	Corner Radius
$1000 \leq Re \leq 2000$	$4mm \leq D \leq 8mm$	$1.5mm \leq r \leq 4mm$

2.2 Thermal Parameters

There are several assumptions that need to be made before the thermal characteristics of the cold plate can be modelled. These assumptions are as follows:

- All heat produced is transferred to the TIM, with no losses [23].
- Steady-state heat transfer.[16, 9].
- Steady, incompressible, & laminar flow [17].
- Top plate is insulated [16, 9].

- Radiation and natural convection are negligible [17].

Utilising the above assumptions, a thermal resistance network can be developed which treats each straight channel segment as an individual cell, whilst neglecting bends. Figure 2.1 [22] shows the thermal resistance network for the baseline geometry.

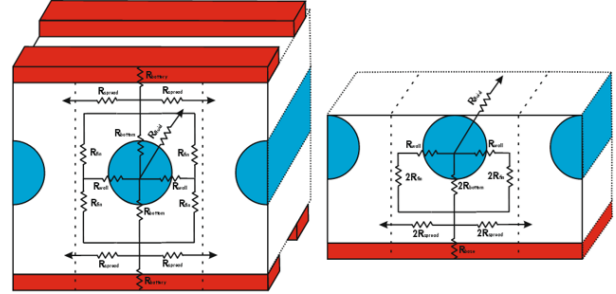


Figure 2.1: Thermal resistance network (left) and a simplified equivalent network (excluding insulated top plate to improve visibility) used for the analysis (right).

The thermal resistance network is made up of a fluid resistance, convective resistances (R_{wall} and R_{bottom}), and conductive resistances (R_{fin} , R_{base} , and $R_{spreading}$). These thermal resistances are combined to give the total thermal resistance. More information on how these thermal resistances were individually calculated is provided in Daniel Nixon's individual report [22].

Another method was developed to calculate the thermal resistance, which is simpler and contains more assumptions. It was found that upon comparison to the validation data, this second method was a much better approximation [22], and so was used in place of the first method described. The added assumptions necessary for this second method are as follows:

- Spreading resistance is negligible.
- General equation negates the requirement of splitting the geometry into segments.

This leads to equation 2.2 being the better alternative for calculating thermal resistance.

$$R_{th} = R_{fluid} + \frac{D_h}{K_f N_u A_{CB}} + \frac{t_b}{K_h WL} \quad (2.2)$$

Using the total thermal resistance, the maximum baseplate temperature is calculated. Equation 2.3 is used for this calculation.

$$T_{b,max} = R_{th} Q + T_{f,in} \quad (2.3)$$

where $T_{f,in}$ is the inlet temperature of the fluid, and Q is the total heat generated, which is calculated using equation 2.4.

$$Q = \dot{m} C_p \Delta T_f \quad (2.4)$$

To calculate the total change in fluid temperature, equation 2.5 is required.

$$\Delta T_f = \frac{q(W_{fin} + W_{ch})}{\dot{m}C_p} L_t \quad (2.5)$$

3. CFD MODELLING

The CFD model developed can predict pressure drop and a range of thermal parameters. The solver settings and boundary conditions are detailed in full, as well as all assumptions made. The mesh design is justified, with a mesh independence study conducted.

3.1 Geometry

The baseline geometry provided by Rolls Royce is displayed in figure 3.1 [24]. The serpentine channel has a diameter of 6mm and a corner radius of 2.5mm. Each battery has an area of 4240mm^2 .

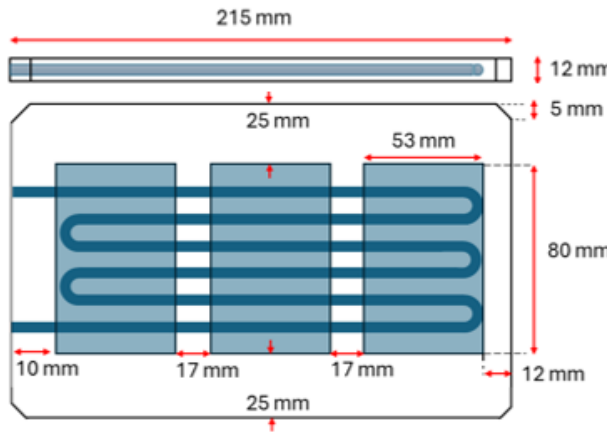


Figure 3.1: Technical drawing of baseline cold plate.

3.2 Solver Settings

Solver settings have been selected based on the paper presented by Imran et al. [10] that is used for validation. The SIMPLE pressure-velocity scheme has been utilised with a least squares cell based solution gradient. As the flow is laminar ($Re < 2000$) the laminar turbulence model has been selected. Second order discretisation schemes have been selected for pressure and momentum to increase accuracy and the simulations are run at double precision to reduce round off error. The following assumptions have been made: the fluid flow is laminar ($Re < 2000$), incompressible and a steady state transport process, the effect of radiation heat transfer is negligible, the influence of gravity and other body forces are neglected and the thermophysical properties of the heat sink and fluid are constant [10]. Table 3.1 [25] shows the solver settings selected.

Table 3.1: Summary of solver Settings [25].

Solver Setting	Selection
Turbulence Model	Laminar
Pressure-Velocity Scheme	SIMPLE
Solution Gradient	Least-Squares Cell Based
Pressure	Second Order Upwind
Momentum	Second Order Upwind

3.3 Boundary Conditions

As inlet velocity must be parameterised this has been set to 'inlet-velocity' and has been adjusted corresponding to each design point. The inlet temperature has been set to 293K and the outlet temperature to 300K. The outlet gauge pressure has been set to 0Pa and each heat source has been assigned a constant heat flux of $94,500\text{ Wm}^{-2}$. The exterior of the cold plate was set to be adiabatic so that the heat transfer in the heat sink is isolated, however in reality some air cooling/radiation would be present [26]. The fluid-pipe wall interaction was set up to be a conjugate/ coupled system. Table 3.2 provides a summary of the boundary conditions used [25].

Table 3.2: Summary of boundary conditions [25].

Boundary	Assigned Parameters
Inlet	'inlet-velocity'. Temperature of 293K.
Outlet	'pressure-outlet'. Gauge pressure 0 Pa. Temperature of 300K.
Wall	Adiabatic

3.4 Mesh Design

The mesh has been designed with an unstructured mesh for the cold plate (solid domain) and a structured mesh for the fluid channel (liquid domain). This was done as the solid domain geometry is more complex and so a structured mesh was not feasible, whereas the fluid domain geometry is consistent and allowed for a structured mesh to be utilised. Figure 3.2 shows a photo of the entire mesh design, where the unstructured solid domain can be clearly observed. This figure also shows a side on view of the geometry, where the inlet and outlet have a structured mesh, and the cold plate has an unstructured mesh.

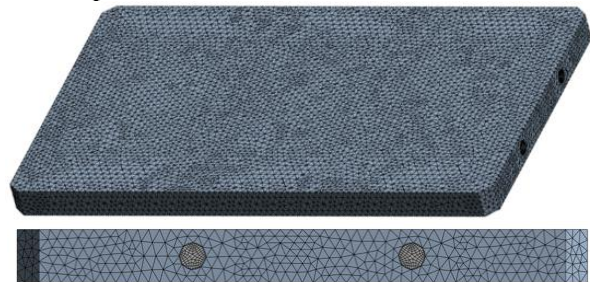


Figure 3.2: Photo of entire mesh (top) of 246267 elements and side on view of mesh (bottom).

The quality of the mesh used for the solid domain is within acceptable limits [27]. The average skewness value is 0.7924 for this part of the mesh. The structured mesh used for the fluid domain has a lower average skewness value of 0.4091 and is more computationally efficient. Figure 3.3 [25] displays the fluid domain mesh only.

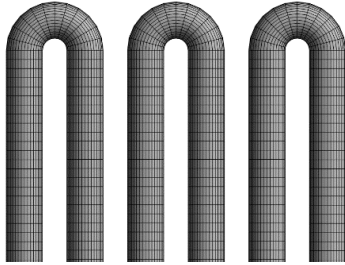


Figure 3.3: Structured mesh for fluid domain [25].

Due to the high computational cost of three dimensional CFD simulations local mesh refinement has not been possible for this model. Local mesh refinement can allow for flow features to be observed more easily but considerably increases the number of elements in the mesh, thus greatly increasing the time taken for each simulation to run. As this project requires that over 100 simulations must be run, this would not be feasible. In addition, the parameterisation of the model makes it difficult to achieve consistent refinement over a range of geometries and thus local mesh refinement would not be practical [25].

To select a mesh with a suitable number of elements a mesh independence test has been carried out for the baseline geometry for maximum base plate temperature and pressure drop at different Reynolds numbers, for a coarse, medium and fine mesh. These are displayed in figure 3.4.

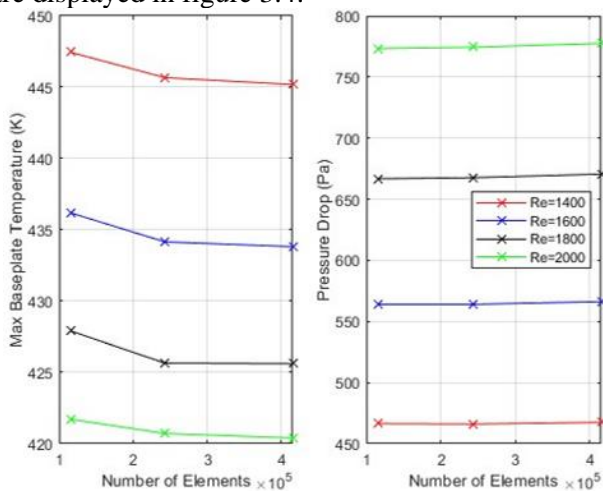


Figure 3.4: Pressure drop and thermal resistance mesh convergence graphs for 4 different Reynolds number.

From the mesh independence test the medium mesh has been selected. For maximum base plate

temperature and pressure drop the maximum percentage difference between the medium and fine mesh is 0.11% and 0.44% respectively. Thus, the medium mesh is deemed suitable. Selecting the medium mesh roughly halves computational cost which is particularly advantageous for optimisation projects like this one, with a large number of design points. As the model must be parameterised the mesh has been designed by assigning element size, which remains the same for each design point. Thus, although the geometry changes with each design point the refinement of the mesh remains the same. The final mesh design is displayed in figure 3.3 [25].

3.5 Parametrisation

To increase the rate at which a CFD simulation can be prepared, parameterisation of the processes prior to analysis were implemented. The settings that remained constant across all the design points did not require parameterisation but the independent variables such as the channel geometry and fluid properties benefited greatly from parameterisation. Since over 100 individual simulations needed to be analysed, the time saving was greatly appreciated. A downside to parameterising is that a pre-selected number of simulation iterations must be applied to all design points. If too few iterations are used, the simulations might not be fully converged for all design points [24]. Too many iterations and the simulation will likely be converged but at the cost of time and resources[24]. In this project, a few random design points were selected and simulated with a different number of iterations selected. The purpose is to evaluate the fewest number of iterations that produces convergence. 10 design points were simulated at a lower (600 iterations, residuals at $1E-08$) and a higher level of accuracy (2000 iterations, residuals at $1E-016$). The maximum difference was 0.011% [24].

4. VALIDATION

A cross validation approach was adopted for this investigation. First, both the analytical and CFD models were validated against experimental and simulation data from Imran et al [10]. Following this, all optimisation work was completed using both models, as a method of cross-checking data. The study from Imran et al [10] investigates and compares different channel configurations for cold plates and was chosen to validate against due to similarities in geometry between configuration A and the baseline geometry. Figure 4.1 [22] highlights the differences between the two geometries.

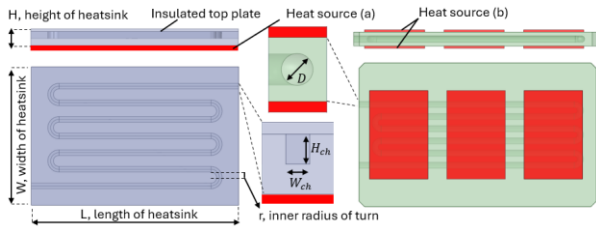


Figure 4.1: Diagram comparing configuration A (left) by Imran et al against the baseline geometry (right).

Figure 4.2 [22] shows the pressure drop and thermal resistance validation results.

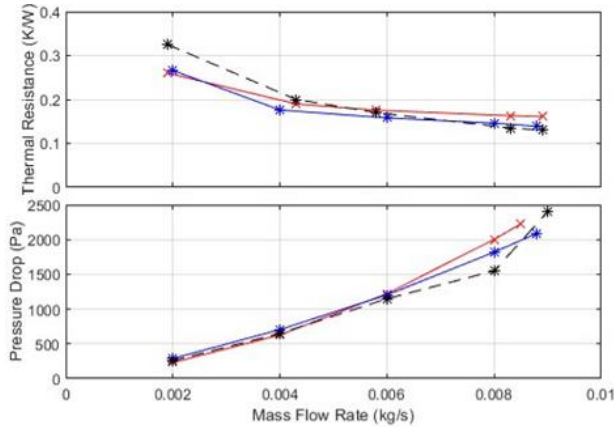


Figure 4.2: Graphs comparing pressure drop (bottom) and thermal resistance (top) data for the validation geometry from the Analytical (red) Model, CFD (blue) model, and Experimental Validation (black).

From figure 4.2, it is observed that all three data sets show the same trend across the range of mass flow rates investigated for the pressure drop. The analytical model agrees closely with the experimental data, with an exception at a mass flow rate of 0.008 kg/s, which is likely due to an experimental anomaly. The CFD data underpredicts pressure drop across the range of investigated mass flow rates, and so an offset factor is applied which multiplies all data points by 2.2. This correction factor is necessary to account for the laminar simulation underpredicting frictional losses throughout the channel.

For the thermal resistance validation, the CFD and experimental data show the same relationship against mass flow rate, with the CFD data being offset by 0.09 consistently across the full range of investigated mass flow rates, and so an offset factor of the same magnitude is applied. The analytical data shows a slightly less sensitive relationship to mass flow rate in comparison to the CFD and experimental data. It initially underpredicts the experimental data at the lowest mass flow rate of 0.002 kg/s by 0.065, is then equal at a mass flow rate of 0.005 kg/s, and finally overpredicts by 0.031 at the highest mass flow rate of 0.009 kg/s.

5. OPTIMISATION

This section details the optimisation of a serpentine channel heatsink, aiming to minimise both pressure drop and thermal resistance. By utilising computational tools like MATLAB, design spaces encompassing pipe diameter, serpentine corner radius, and Reynolds number will be explored. The optimisation problem is as follows:

Minimise: $f(D, r, Re) = (R_{th}(D, r, Re), \Delta P(D, r, Re))$

Subject to: $4mm \leq D \leq 8mm$

$1.5mm \leq r \leq 4mm$

$1000 \leq Re \leq 2000$

Figure 5.1 [28] shows the workflow for the optimisation which was introduced in chapter 1.

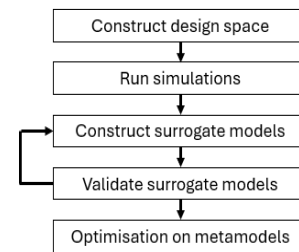


Figure 5.1: Optimisation workflow [28].

5.1 Design Space Generation

A design space is a conceptual domain in which solutions are generated for a specific problem. The design space needs to encompass the constraints each variable must adhere to all while exploring the possibilities across the entire range. An initial design space comprising of 100 design variables was created utilising the Morris-Mitchell Latin Hypercube sampling technique. The Latin hypercube method partitions the range of each input design variable into uniform intervals and subsequently selects a random value from each interval for every factor, this method is highly efficient [29]. To ensure accuracy when meta modelling, the Morris Mitchell condition guarantees optimal coverage of the design space.

As the work carried out incorporates both an analytical model as well as a higher fidelity CFD model, the design space began extremely large (table 2.2) then was reduced in size. The analytical model can simulate a larger quantity of design points in a short amount of time however this is not possible for CFD models. The original 100-point analytical design space coupled with the reduced 27-point CFD design space is shown in figure 5.2 [28], rationale for reducing the design space is proposed in [28].

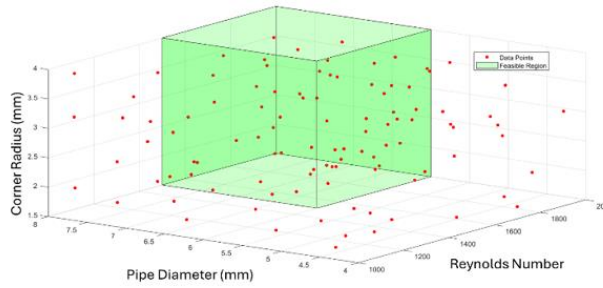


Figure 5.2: The design space with reduced region highlighted in green [28].

5.2 Surrogate Modelling

For the construction of the surrogate models, a value can be attributed representing both pressure drop and thermal resistance for each of the design points in each of the design spaces, which serve as the objective functions. These simulated data points then form the training set for the construction of a surrogate model. In this case, Gaussian radial basis functions are employed in the construction of the surrogate models. Once trained, the surrogate models act as efficient approximations of the interplay between the design variables and objective functions. This enables rapid exploration of the design space during optimisation processes. This is summarised in figure 5.3 [28].



Figure 5.3: Process for the creation of a surrogate model.

To refine the accuracy of the metamodels, machine learning techniques were employed, specifically K-Fold Cross Validation. Ultimately, K-Fold Cross Validation ensures the metamodel's reliability and robustness across different datasets, enhancing confidence in the optimisation processes. This is further explored in [28].

5.3 Single Objective Optimisation

Single Objective Genetic Algorithms (SOGAs) are optimisation algorithms that mimic natural selection processes to find optimal solutions to single-objective optimisation problems. While SOGAs may not directly optimise multiple objectives simultaneously, they provide valuable insights into the problem space and facilitate informed decision-making. Before proceeding with multi-objective optimisation, a total of eight single-objective optimisations were conducted. Each two variable design space was

minimised for both pressure drop and thermal resistance separately. Additionally, both the analytical model and the CFD model were utilised for running all four single-objective optimisations, with the CFD model being employed on the reduced design spaces resulting from the preliminary analysis.

Table 5.1: Single objective minima predictions for a constant pipe diameter [28].

Constant Pipe Diameter (6mm)			
Analytical			
Reynolds Number	Corner Radius (mm)	Pressure Drop (Pa)	Thermal Resistance (°C/W)
1505.1	3.9748	851.8262	
2000	2.7749		0.1166
CFD			
Reynolds Number	Corner Radius (mm)	Pressure Drop (Pa)	Thermal Resistance (°C/W)
1505.1	3.5585	1028.7	
2000	3.656		0.1251

Table 5.2: Single objective minima predictions for a constant corner radius [28].

Constant Corner Radius (2.5mm)			
Analytical			
Reynolds Number	Pipe Diameter (mm)	Pressure Drop (Pa)	Thermal Resistance (°C/W)
1515.2	7.9696	445.0443	
2000	7.4152		0.1164
CFD			
Reynolds Number	Corner Radius (mm)	Pressure Drop (Pa)	Thermal Resistance (°C/W)
1512.2	7.9596	523.3890	
1980.4	7.3213		0.1202

The conclusion of multiple single-objective optimisation algorithms provided significant insights into parameter dependencies, which are further detailed in Aaron's individual report [28]. A comparison between the two modelling techniques also revealed the following:

- The analytical model consistently forecasts higher values of pressure drop and thermal resistance across all evaluations.
- The analytical model demonstrates relatively low sensitivity to changes in corner radius and pipe diameter, as highlighted in Dan's individual report.

Shifting the focus towards the interplay between design parameters and objectives, the single-objective optimisations provide valuable insights. Reynolds number emerges as a significant influencer on both objectives compared to structural parameters,

underscoring the importance of flow characteristics. Additionally, it became evident that smaller pipe diameters and corner radii led to considerable increases in pressure drop. This increase is due to the increased frictional resistance because of both the increase in velocity of the coolant and proportion of the fluid in contact with the channel walls. This also attributes to the increase in thermal resistance.

5.4 Multi Objective Optimisation

Multi-objective optimisation is subsequently applied to the design space comprising of three variables for both the analytical and CFD models. Multi-objective genetic algorithms (MOGAs) are specialized optimisation algorithms designed to handle problems with multiple conflicting objectives. Unlike SOGAs, MOGAs evaluate solutions based on vectors of objective function values, aiming to approximate the Pareto front where no solution dominates another in all objectives. The Pareto front, often referred to as the Pareto boundary or Pareto set, highlights the optimal solutions within a multi-objective optimisation scenario. Normalization fosters fairness and comparability in data analysis, paving the way for more reliable and interpretable results. Figure 5.5 [28] shows the Pareto fronts produced from the CFD and analytical models.

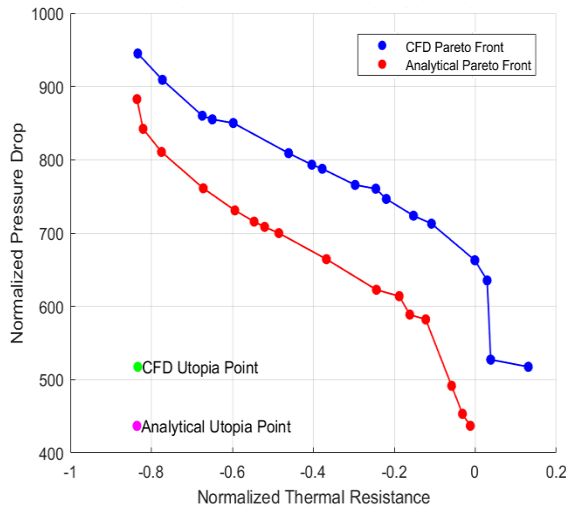


Figure 5.5: Pareto fronts of Non-Dominated Solutions.

Analysing the Pareto front provides valuable insights into the optimal compromises between various design criteria. This information enables informed decision-making about the design space, helping to identify solutions that strike the best balance across both objectives. Exploring different sections of the Pareto front allows designers to grasp the implications of prioritizing one objective over another. In this specific Pareto front, it highlights the trade-offs between thermal resistance and pressure

drop, the visualization reveals that with a small thermal resistance comes a large pressure drop and vice versa.

6. DISCUSSION

To verify the accuracy of the metamodels, the design points generated from the single-objective optimisations were re-simulated using both CFD and the analytical model. Subsequently, the objective functions were compared against the predictions made by the metamodels, detailed in Aaron's individual report [28].

Table 6.1: Error in surrogate model predictions [28].

Metamodel Type	Average Error (%)
Pressure Drop	1.75
Thermal Resistance	0.70

Table 6.1 underscores the precision of the metamodels, revealing minimal discrepancies between predicted and actual values. The larger error evident in the pressure drop modelling is likely attributed to the broader range of pressure drop values compared to the narrower range of thermal resistance.

The generated Pareto sets for both models were subsequently assessed. By simulating the corresponding three-dimensional design points for each Pareto optimal solution, the interaction between pressure drops and thermal parameters became evident. Given that one of the heatsinks conditions is to maintain the base plate temperature below 396K, maximum base plate temperature became an additional objective of interest. Figure 6.1 [28] illustrates the relationship between pressure drop and maximum base plate temperature for the re-simulated Pareto sets.

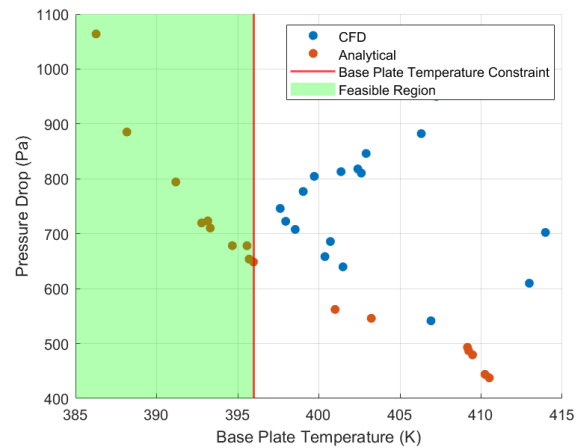


Figure 6.1: Pareto optimal solutions from CFD and analytical model with feasible region highlighted green.

Figure 6.1 indicates that the desired base plate temperature is only attained for the analytical model. However, the accuracy of the model's prediction of

thermal resistance is questionable. High-fidelity CFD simulations reveal that achieving a base plate temperature below 396K is unattainable. This suggests that Rolls Royce cannot achieve their desired cooling solely by focusing on flow characteristics and heatsink structure. Therefore, an exploration of the use of gyros or additional flow disruption techniques should be considered. These sort of techniques will induce additional mixing, thereby disrupting the thermal boundary layer and increasing the heat transfer rate which will result in a lower thermal resistance and peak baseplate temperature [30]. While not meeting the stringent threshold set by Rolls Royce, figure 6.1 demonstrates successful optimisation. Given the prioritization of thermal resistance, the Pareto optimal solution produced by CFD, just to the right of the base plate temperature constraint, is considered optimal (table 6.2).

Table 6.2: Optimal compromise point data [28].

Re	D (mm)	r (mm)	Pressure Drop (Pa)	Base Plate Temperature (K)
1893.07	7.95	2.66	746.03	397.62

Comparing the results of the newly optimised design with the baseline, it can be seen there is an 48.97% and 13.83% decrease in pressure drop and baseplate temperature respectively (table 6.3 [28]).

Table 6.3: Optimised and baseline design comparison.

Model	Pressure Drop (Pa)	Base Plate Temperature (K)
Baseline	1461.88	461.46
Optimised Design	746.03	397.62
% improvement	48.97 %	13.83 %

7. CONCLUSION

The set of design variables selected for the investigation varied in sensitivity to the optimisation objectives. Reynolds number was the most significant to both pressure drop and thermal resistance. Despite the geometric variables (channel diameter and corner radius) being less impactful on performance, we did improve the baseline geometry design significantly (at constant Reynolds number), reducing the pressure drop and thermal resistance by 48.97% and 13.83%. In summary, the set of optimal designs which make up the Pareto front are not able to meet the requirement set by Rolls Royce of a maximum baseplate temperature of 396K. If more complex geometric variables were used, such as gyros which would induce additional mixing, the subsequent disruption to the thermal boundary layer would decrease the thermal resistance thus potentially meeting the baseplate temperature criteria.

Incorporating more complex design variables like this in the optimisation problem could lead to a design that satisfies the requirements set by Rolls Royce.

7.1 Achievements and Impact

The aim set at the beginning of this project was met. The following achievements are highlighted:

1. Produced a Pareto front of designs that trade off pressure drop and thermal performance.
2. Created a fully parameterized CFD model that can be reused for further analysis.
3. Gained an understanding of how the design variables affect cold plate performance.

7.2 Future Work

For future work, the thermal resistance analytical model should be further developed so that it is sensitive to more design variables. Also, a separate CFD model for the pressure loss would be ideal, as the heat transfer is assumed laminar. This separate model could utilise a turbulence model to predict the pressure loss more accurately. Finally, modelling more complex geometric features that would induce mixing should be investigated.

ACKNOWLEDGEMENTS

We would like to thank Professor Harvey Thompson for the support and expert advice he provided throughout the duration of this project.

REFERENCES

- [1] Anon n.d. Aviation. *IEA*. [Online]. [Accessed 14 March 2024a]. Available from: <https://www.iea.org/energy-system/transport/aviation>.
- [2] Anon 2022b. The aviation sector wants to reach net zero by 2050. How will it do it? *World Economic Forum*. [Online]. [Accessed 14 March 2024]. Available from: <https://www.weforum.org/agenda/2022/12/aviation-net-zero-emissions/>.
- [3] Canders, W.-R., Hoffmann, J. and Henke, M. 2019c. Cooling Technologies for High Power Density Electrical Machines for Aviation Applications. *Energies*. **12**(23), p.4579.
- [4] Sharma, A., Capoor, G.K. and Chattopadhyay, A.B. 2015d. Advanced aircraft electrical systems to enable an All-Electric aircraft In: *2015 International Conference on Electrical Systems for Aircraft, Railway, Ship Propulsion and Road Vehicles (ESARS)* [Online]., pp.1–6. [Accessed 6 November 2023]. Available from: <https://ieeexplore.ieee.org/abstract/document/7101423>.
- [5] Anon n.d. Thermal Control. *Glenn Research Center / NASA*. [Online]. [Accessed 14 March 2024e]. Available from:

- <https://www1.grc.nasa.gov/aeronautics/eap/technology/energy-efficient-technology/thermal-control/>.
- [6] Deisenroth, D.C. and Ohadi, M. 2019f. Thermal Management of High-Power Density Electric Motors for Electrification of Aviation and Beyond. *Energies*. **12**(19), p.3594.
- [7] Wang, J., Li, Y., Liu, X., Shen, C., Zhang, H. and Xiong, K. 2021g. Recent active thermal management technologies for the development of energy-optimized aerospace vehicles in China. *Chinese Journal of Aeronautics*. **34**(2), pp.1–27.
- [8] December 2012, E.E.M. | N. n.d. Thermal Management. *Aerospace Manufacturing and Design*. [Online]. [Accessed 14 March 2024h]. Available from: <https://www.aerospacemanufacturinganddesign.com/article/amd1212-electronics-thermal-management/>.
- [9] Hao, X., Peng, B., Xie, G. and Chen, Y. 2014i. Thermal Analysis and Experimental Validation of Laminar Heat Transfer and Pressure Drop in Serpentine Channel Heat Sinks for Electronic Cooling. *Journal of Electronic Packaging*. **136**(3), p.031009.
- [10] Imran, A.A., Mahmoud, N.S. and Jaffal, H.M. 2018j. Numerical and experimental investigation of heat transfer in liquid cooling serpentine mini-channel heat sink with different new configuration models. *Thermal Science and Engineering Progress*. **6**, pp.128–139.
- [11] Coutinho, M., Bento, D., Souza, A., Cruz, R., Afonso, F., Lau, F., Suleman, A., Barbosa, F.R., Gandolfi, R., Affonso, W., Odaguil, F.I.K., Westin, M.F., Dos Reis, R.J.N. and Da Silva, C.R.I. 2023k. A review on the recent developments in thermal management systems for hybrid-electric aircraft. *Applied Thermal Engineering*. **227**, p.120427.
- [12] Sameer Mahmoud, N., Mohammad Jaffal, H. and Abdulnabi Imran, A. 2021l. Performance evaluation of serpentine and multi-channel heat sinks based on energy and exergy analyses. *Applied Thermal Engineering*. **186**, p.116475.
- [13] Al-Neama, A.F.M. n.d. Serpentine Minichannel Liquid-Cooled Heat Sinks for Electronics Cooling Applications.
- [14] Li, X., Hao, X., Chen, Y., Zhang, M. and Peng, B. 2013n. Multi-Objective Optimizations of Structural Parameter Determination for Serpentine Channel Heat Sink In: Esparcia-Alcázar, A. I. ed. *Applications of Evolutionary Computation*. Lecture Notes in Computer Science. Berlin, Heidelberg: Springer Berlin Heidelberg, pp.449–458.
- [15] Ismaeel, M.E., Kapur, N., Khatir, Z. and Thompson, H.M. 2021o. Robust Optimisation of Serpentine Fluidic Heat Sinks for High-Density Electronics Cooling In: Wen, C. and Yan, Y. eds. *Advances in Heat Transfer and Thermal Engineering*. Singapore: Springer Singapore, pp.583–590.
- [16] Tsai, T.-H. and Chein, R. 2012p. Simple model for predicting microchannel heat sink performance and optimization. *Heat and Mass Transfer*. **48**(5), pp.789–798.
- [17] Hao, X.-H., Li, X.-K., Peng, B., Zhang, M. and Zhu, Y. 2014q. Thermal resistance network model for heat sinks with serpentine channels. *International Journal of Numerical Modelling: Electronic Networks, Devices and Fields*. **27**(2), pp.298–308.
- [18] Simpson, T.W., Poplinski, J.D., Koch, P.N. and Allen, J.K. 2001r. Metamodels for Computer-based Engineering Design: Survey and recommendations. *Engineering with Computers*. **17**(2), pp.129–150.
- [19] Sudret, B. 2012s. Meta-models for structural reliability and uncertainty quantification.
- [20] Konak, A., Coit, D.W. and Smith, A.E. 2006t. Multi-objective optimization using genetic algorithms: A tutorial. *Reliability Engineering & System Safety*. **91**(9), pp.992–1007.
- [21] Maharudrayya, S., Jayanti, S. and Deshpande, A.P. 2004u. Pressure losses in laminar flow through serpentine channels in fuel cell stacks. *Journal of Power Sources*. **138**(1–2), pp.1–13.
- [22] Nixon, D. n.d. Analytical Modelling of a Serpentine Channel Cold Plate for Next Generation Aerospace Application. *University of Leeds*.
- [23] Anon 2021w. Numerical and Experimental Study on the Heat Transfer Characteristics in the Minichannel Heat Sinks | Engineering Transactions: A Research Publication of Mahanakorn University of Technology.
- [24] Huckle, L. n.d. Optimisation Of Heat Exchanger Systems For Next Generation Aerospace Vehicles Using Computational Fluid Dynamics. *University of Leeds*.
- [25] Christensen, E. n.d. Computational Fluid Dynamics of Heat Transfer in a Serpentine Channel Heat Sink for Next Generation Aerospace Vehicles. *University of Leeds*.
- [26] Anon 2020z. How to Set the Right Thermal Wall Conditions in CHT. *SimScale*. [Online]. [Accessed 26 April 2024]. Available from: <https://www.simscale.com/knowledge-base/how-to-set-the-right-thermal-wall-conditions-in-cht-without-using-radiation/>.
- [27] Anon n.d. ANSYS FLUENT 12.0 User's Guide - 6.2.2 Mesh Quality. [Accessed 26 April 2024aa]. Available from: <https://www.afs.enea.it/project/neptunius/docs/fluent/html/ug/node167.htm>.
- [28] Racher, A. n.d. Machine Learning-Enabled Multi Objective Optimisation of a Heat Exchanger for Next Generation Aerospace Vehicles. *University of Leeds*.
- [29] Sheikholeslami, R. and Razavi, S. 2017ac. Progressive Latin Hypercube Sampling: An efficient approach for robust sampling-based analysis of environmental models. *Environmental Modelling & Software*. **93**, pp.109–126.
- [30] Raske, N., Ausin Gonzalez, O., Furino, S., Pietropaoli, M., Shahpar, S. and Montomoli, F. 2022ad. Thermal Management for Electrification in Aircraft Engines: Optimization of Coolant System In: *Volume 6B: Heat Transfer — General Interest/Additive Manufacturing Impacts on Heat Transfer; Internal Air Systems; Internal Cooling* Rotterdam, Netherlands: American Society of Mechanical Engineers.